nature portfolio

https://doi.org/10.1038/s41565-021-01019-7

## Supplementary information

# Nanoscale chemical heterogeneity dominates the optoelectronic response of alloyed perovskite solar cells

In the format provided by the authors and unedited

Supplementary Materials for

# Nanoscale Chemical Heterogeneity Dominates the Optoelectronic Response of Alloyed Perovskite Solar Cells

Kyle Frohna, Miguel Anaya*, Stuart Macpherson, Jooyoung Sung, Tiarnan A. S. Doherty, Yu-Hsien Chiang, Andrew J. Winchester, Kieran W.P. Orr, Julia E. Parker, Paul D. Quinn, Keshav M Dani, Akshay Rao, Samuel D. Stranks*

*sds65@cam.ac.uk, ma811@cam.ac.uk

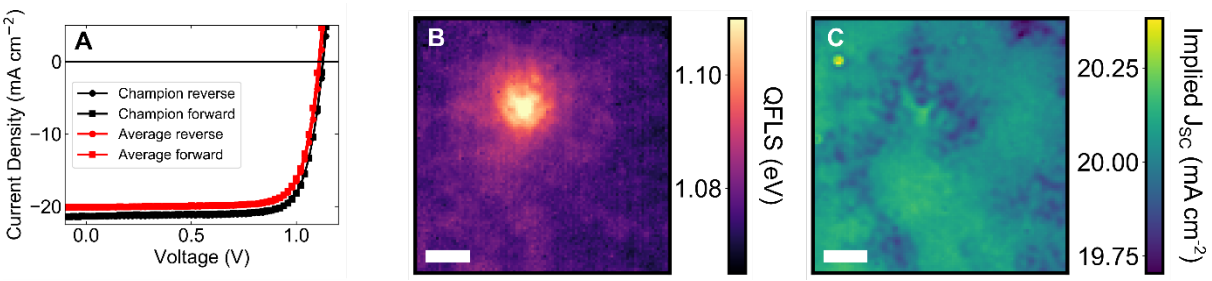


**Supplementary Figure 1: JV curve and maps of a $FA_{0.79}MA_{0.16}Cs_{0.05}Pb(I_{0.83}Br_{0.17})_3$ based p-i-n solar cell stack.** a) Current voltage (JV) curve of a champion p-i-n based solar cell with $V_{OC}$ of 1.12 V, $J_{SC}$ of 21.4 mA/cm$^2$, fill factor of 0.78 and a power conversion efficiency of 18.8% and a JV curve of an average solar cell from the batch with $V_{OC}$ of 1.11 V, $J_{SC}$ of 20.1 mA/cm$^2$, fill factor of 0.78 and a power conversion efficiency of 17.4%. b) QFLS map of a perovskite solar cell device stack. c) Implied $J_{SC}$ map extracted from reflectance maps from the same region extracted in panel B. Scalebars are 5 μm.

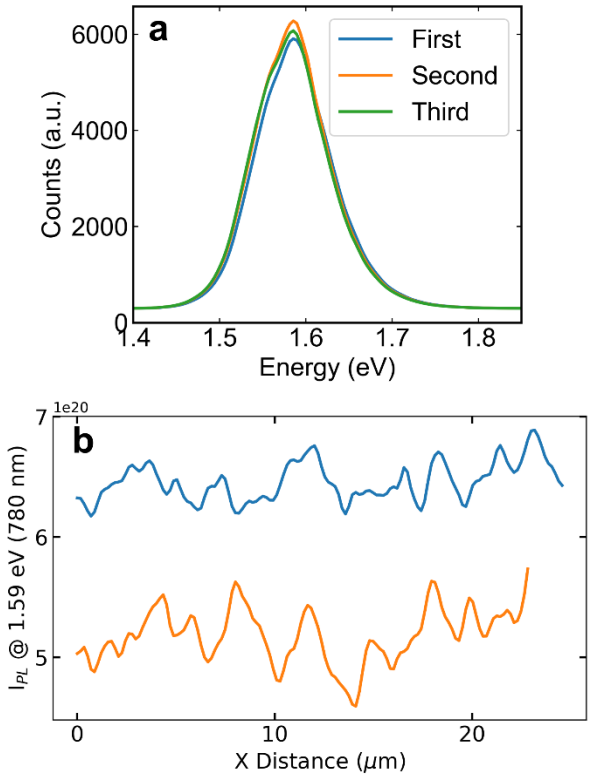


**Supplementary Figure 2: Light soaking stability of $FA_{0.79}MA_{0.16}Cs_{0.05}Pb(I_{0.83}Br_{0.17})_3$ film.** a) The spatially averaged PL spectra of a region of a film mapped repeatedly by the hyperspectral microscope under typical conditions (see Methods). The light dose of 405-nm excitation in each map is ~8 J/cm$^2$. b) The Y-averaged (with respect to camera orientation) variation in PL intensity across the X direction for two different triple cation perovskite samples (blue and orange). The geometry of the setup and the angle of the grating with respect to the incoming PL means that the PL at a given wavelength is effectively measured at earlier times on the right hand side of the sample and at later times on the left. If photobrightening and/or phase segregation dominated the optoelectronic variation we see during our measurement, we would expect to see an increase in PL from the right to the left of the sample. Given that we do not see any significant trend from right to left, we believe the sample is not changing significantly over the course of the measurement.

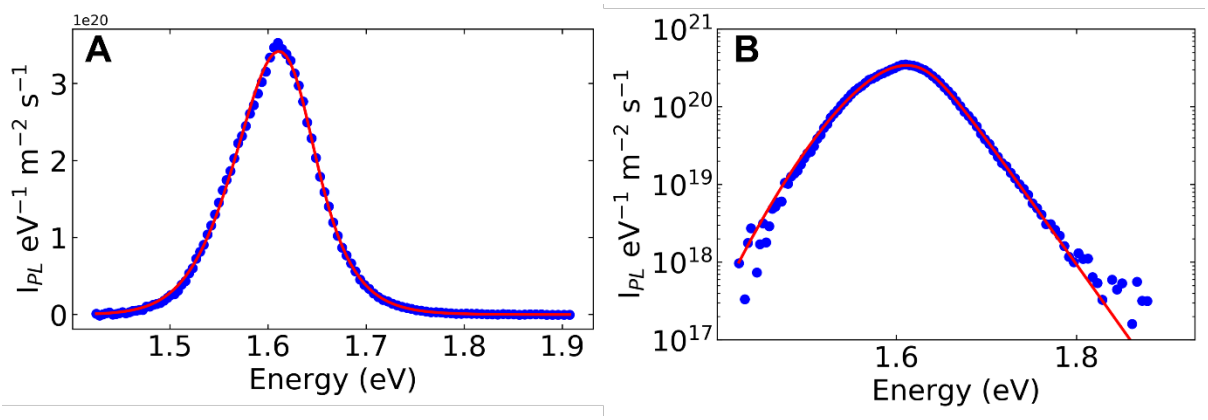


**Supplementary Figure 3: Full Peak Fitting of PL spectra.** PL spectra (blue circles) from a randomly chosen pixel of a map of a $FA_{0.79}MA_{0.16}Cs_{0.05}Pb(I_{0.83}Br_{0.17})_3$ film overlaid with the full peak Planck's law fit plotted in a a) linear and b) logarithmic y axis. The fitted parameters for this spectrum were $\Delta\mu$ =1.233 eV, $\gamma$ = 0.034 eV, $\theta$ =1.413 and $E_g$=1.627.

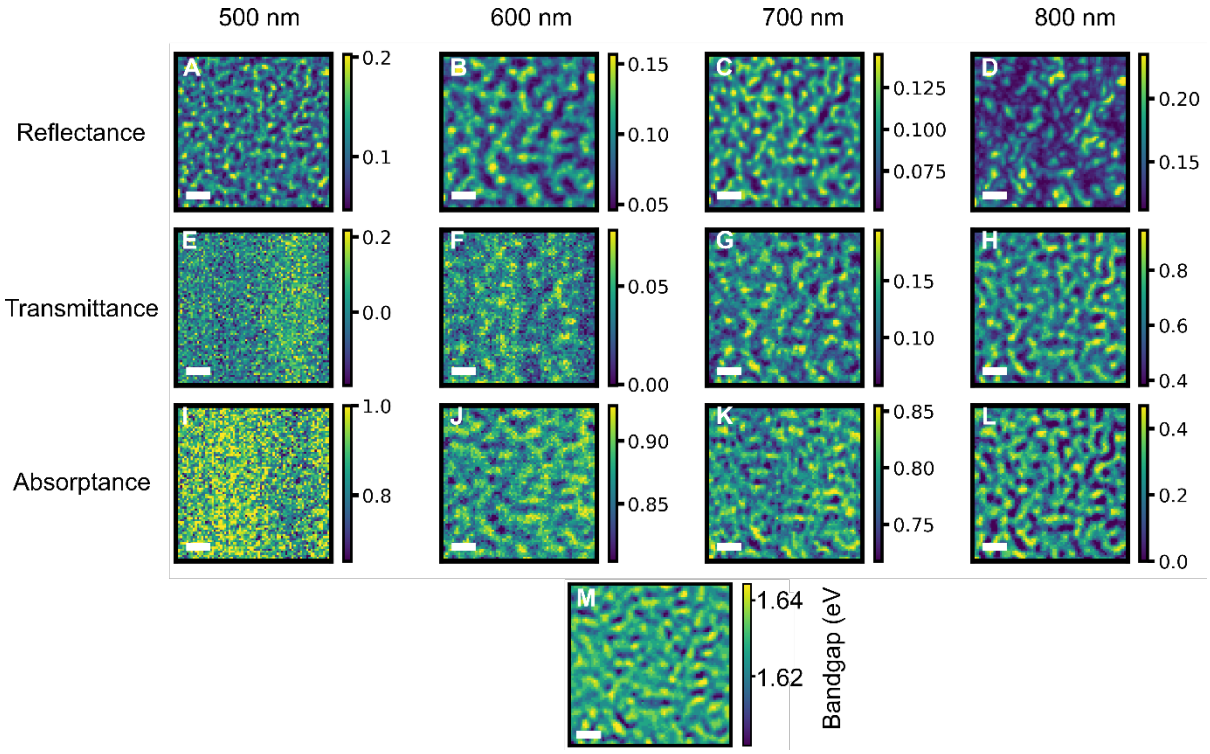


**Supplementary Figure 4: Reflectance, transmittance and absorptance maps of a $FA_{0.79}MA_{0.16}Cs_{0.05}Pb(I_{0.83}Br_{0.17})_3$ perovskite thin film.** Absolute reflectance maps at a) 500 nm, b) 600 nm, c) 700 nm and d) 800 nm respectively. Absolute transmittance maps at e) 500 nm, f) 600 nm, g) 700 nm and h) 800 nm respectively. Absolute absorptance maps at i) 500 nm, j) 600 nm, k) 700 nm and l) 800 nm respectively. m) The optical bandgap (energy at which absorptance drops below 0.5) extracted from the 1-R-T measurements above. All scalebars are 2 μm.

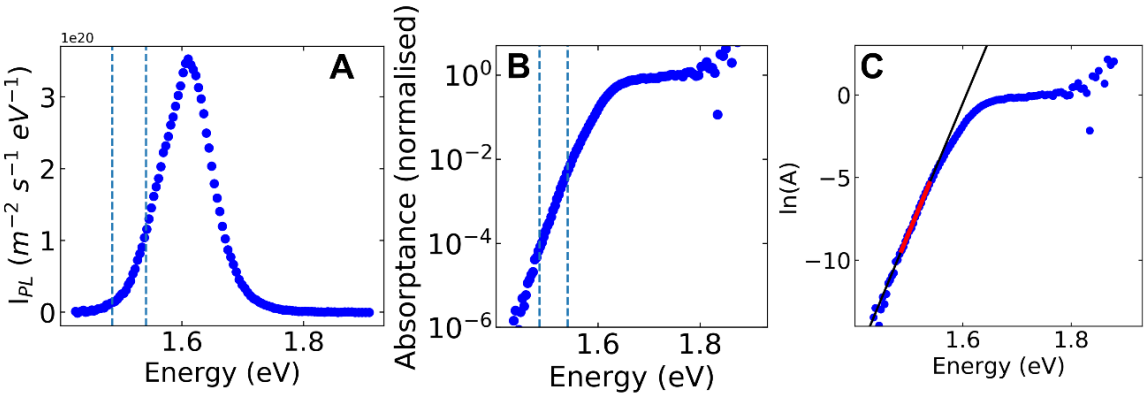


**Supplementary Figure 5: Low energy tail fitting for Urbach energy extraction.** a) PL spectrum of the same randomly chosen pixel of a map of a $FA_{0.79}MA_{0.16}Cs_{0.05}Pb(I_{0.83}Br_{0.17})_3$ shown in figure S1. b) The absorptance spectrum extracted from the PL spectrum shown in panel a). c) The natural log of the absorptance spectrum, allowing the fitting of a linear region (red line) to extract an Urbach energy of 12.7 meV for this point.

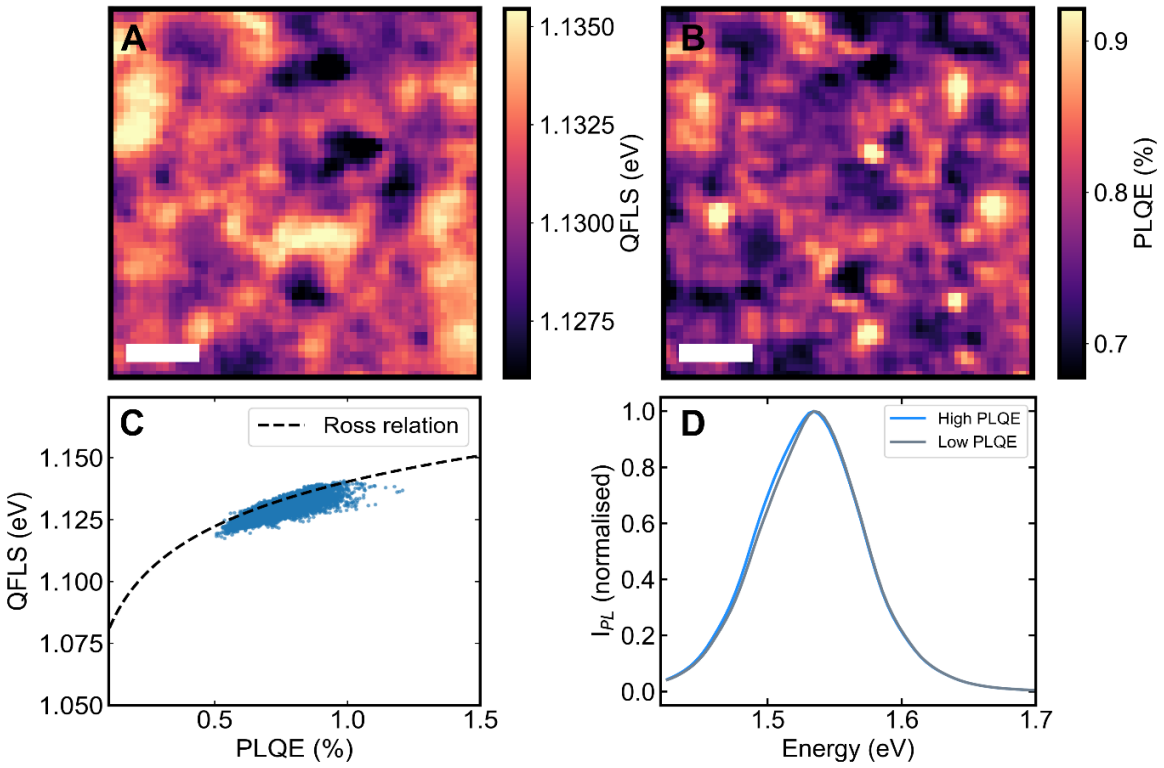


**Supplementary Figure 6: Hyperspectral PL maps of $FA_{0.79}MA_{0.16}Cs_{0.05}PbI_3$ perovskite thin film.** a) QFLS and b) PLQE maps of a $FA_{0.79}MA_{0.16}Cs_{0.05}PbI_3$ perovskite film. Scalebars are 2 μm. c) Scatter plot of the QFLS versus the PLQE overlaid with the Ross relation function assuming a radiative limit of 1.26 eV. d) The PL spectra of the >80$^{th}$ percentile (blue line) and <20$^{th}$ percentile PLQE regions showing negligible difference compared to the mixed halide case.

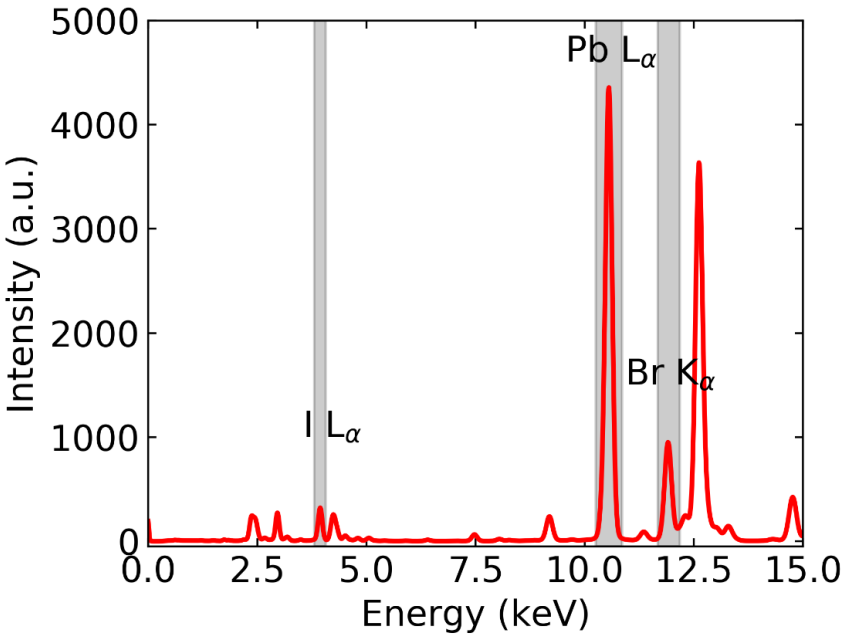


**Supplementary Figure 7: XRF spectrum of $FA_{0.79}MA_{0.16}Cs_{0.05}Pb(I_{0.83}Br_{0.17})_3$ perovskite thin film.** Summed nXRF spectrum of a representative area of a $FA_{0.79}MA_{0.16}Cs_{0.05}Pb(I_{0.83}Br_{0.17})_3$ perovskite thin film. Highlighted are the I $L_\alpha$, Pb $L_\alpha$ and the Br $K_\alpha$ characteristic XRF lines used for analysis.

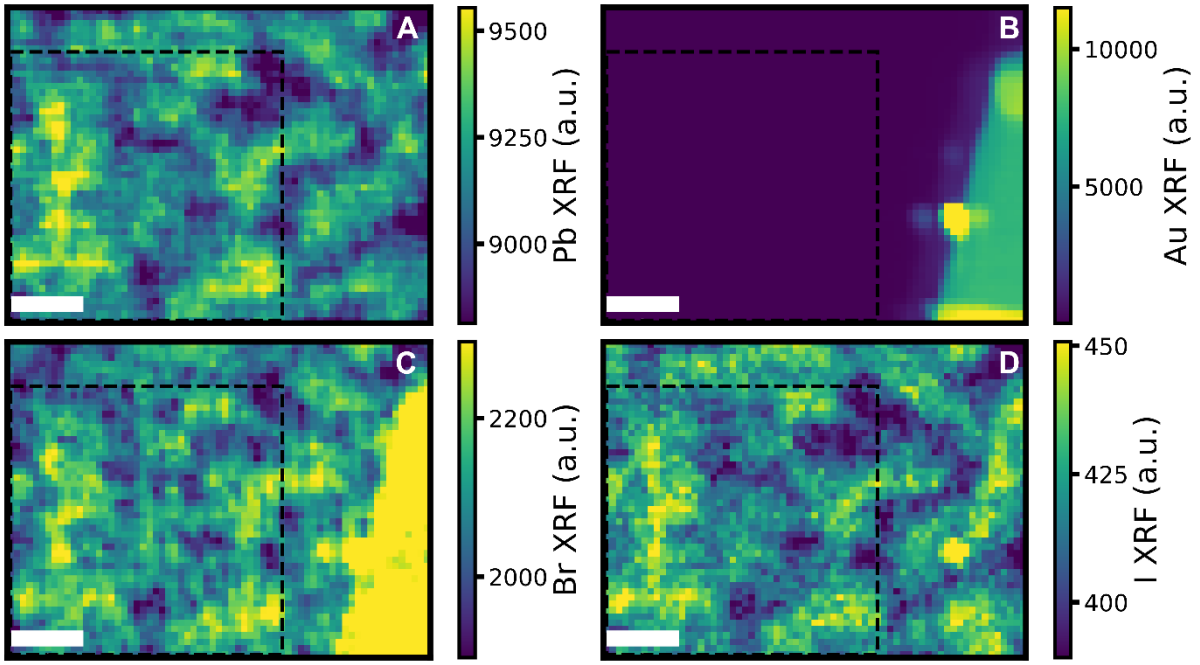


**Supplementary Figure 8: Elemental nXRF maps of $FA_{0.79}MA_{0.16}Cs_{0.05}Pb(I_{0.83}Br_{0.17})_3$ perovskite film.** a) nXRF intensity map of Pb L line. b) nXRF intensity map of the Au L line from the gold fiducial markers used for spatial correlations. c) nXRF intensity map of the Br K line. d) nXRF intensity map of the I L line. The black dashed box indicates the region used for analysis in figure 2 of the main text. All scale bars are 2 μm.

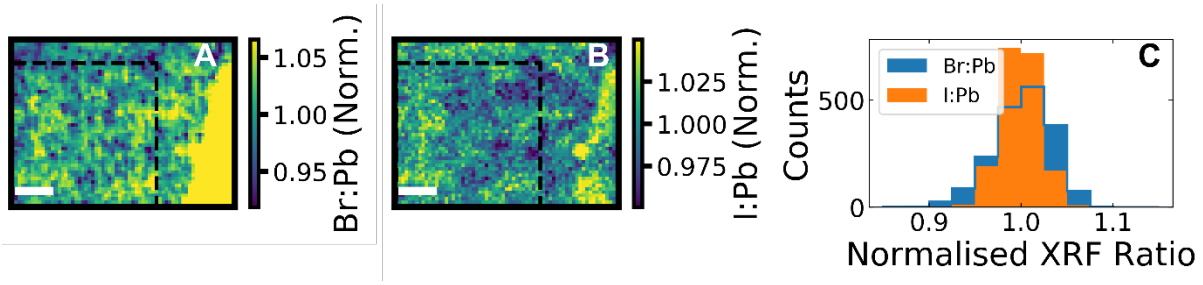


**Supplementary Figure 9: nXRF Ratio maps of $FA_{0.79}MA_{0.16}Cs_{0.05}Pb(I_{0.83}Br_{0.17})_3$ perovskite film.** (A) Normalised Br:Pb nXRF intensity ratio map. (B) Normalised I:Pb nXRF intensity ratio map. (C) Histogram of the Br:Pb and I:Pb ratios from the two maps in the area enclosed by the dashed black square highlighting the greater spread in Br:Pb ratio. All scalebars are 2 μm.

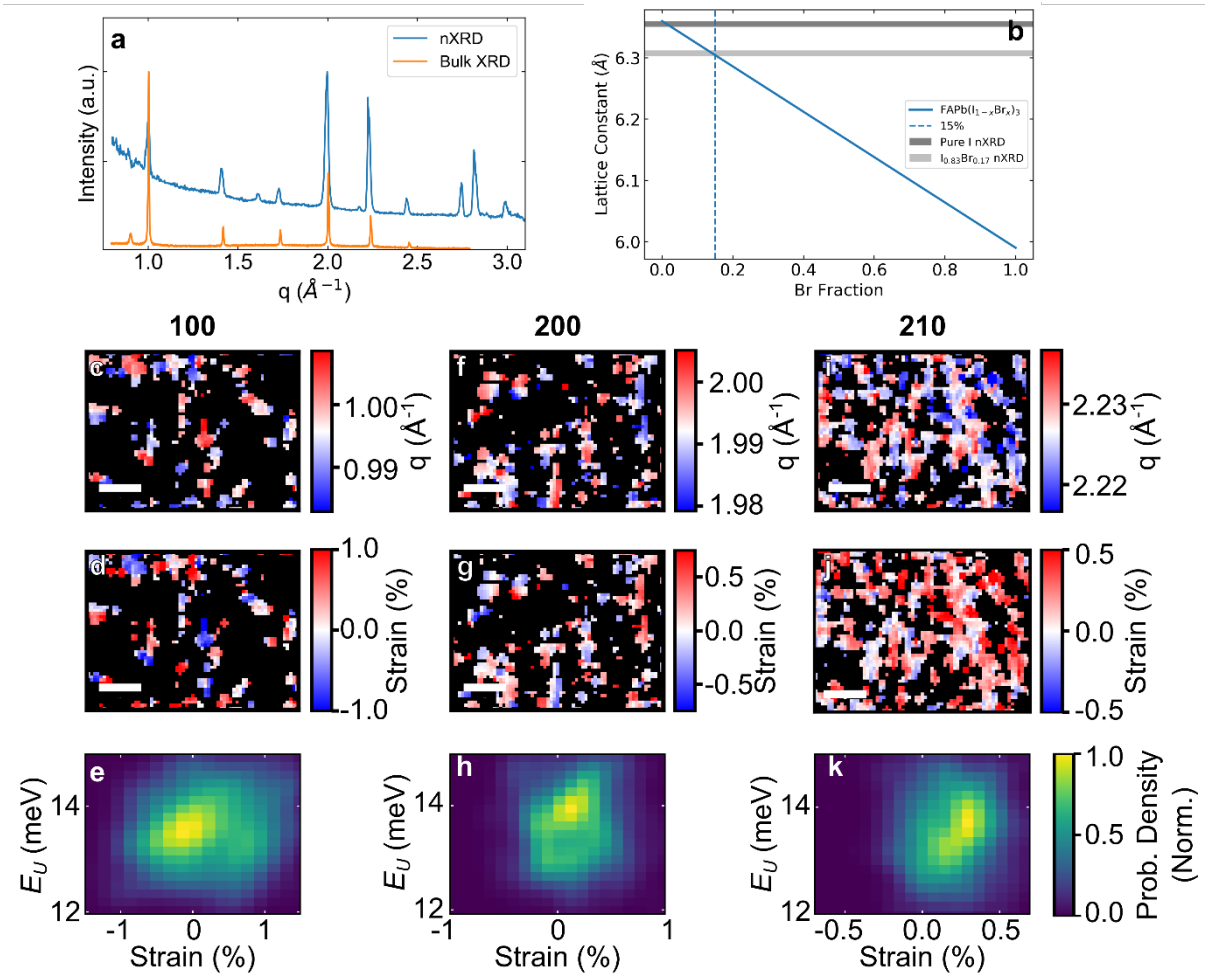


**Supplementary Figure 10: Bulk XRD and nXRD on $FA_{0.79}MA_{0.16}Cs_{0.05}Pb(I_{0.83}Br_{0.17})_3$ films.** a) Bulk XRD spectrum (orange line) and summed nXRD spectrum of representative perovskite films showing that the nXRD spectrum matches well with bulk measurements and confirms that our nXRF measurements remain valid irrespective of potential beam damage. b) Vegard's law extrapolation of the lattice constant as a function of Br content for the model $FAPb(I_{1-x}Br_x)_3$ system, overlaid by the lattice constant extracted from the mean nXRD peak positions of the pure iodide ($FA_{0.79}MA_{0.16}Cs_{0.05}PbI_3$, dark grey) and mixed halide ($FA_{0.79}MA_{0.16}Cs_{0.05}Pb(I_{0.83}Br_{0.17})_3$,light grey). Blue dashed line denotes the effective composition of 15%, close to the approximation of 17% used for the full triple cation experimental system. c) Peak shift map and d) strain map of the {100} family of planes (mean value of 0.11%). e) 2-D kernel density estimation plot of $E_U$ versus strain along the {100} family of planes showing a weak positive correlation(Spearman's r value =0.135, p-value = $2.8\times10^{-4}$). f) Peak shift map and g) strain map of the {200} family of planes (mean value of 0.08%). h) 2-D kernel density estimation plot of $E_U$

versus strain along the {200} family of planes showing no significant correlation (Spearman's r value =0.05, p-value = 0.12). i) Peak shift and j) strain map of the {210} family of planes (mean value of 0.15%) corresponding to the maps shown in the main text in figure 3. k) 2-D kernel density estimation plot of $E_U$ versus strain along the {210} family of planes showing a weak positive correlation (Spearman's r value =0.07, p-value = $4\times10^{-3}$). All scalebars are 2 μm.

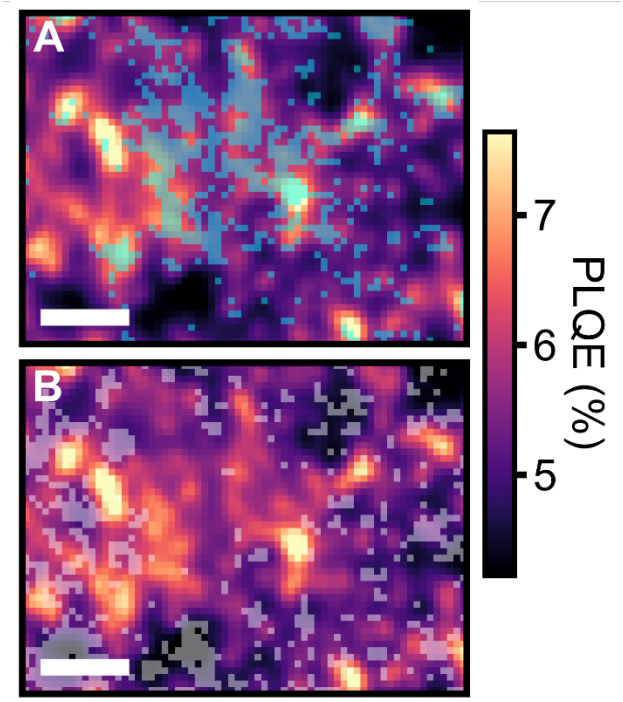


**Supplementary Figure 11: PLQE maps of triple cation perovskite film overlaid with high and Br:Pb regions.** a) PLQE map overlaid with the high Br:Pb regions (>80$^{th}$ percentile) and b) low Br:Pb regions (<20$^{th}$ percentile). These are the same areas shown in the main text in Figure 3 and correspond to the histogram in Figure 3e. Scalebars are 2 μm.

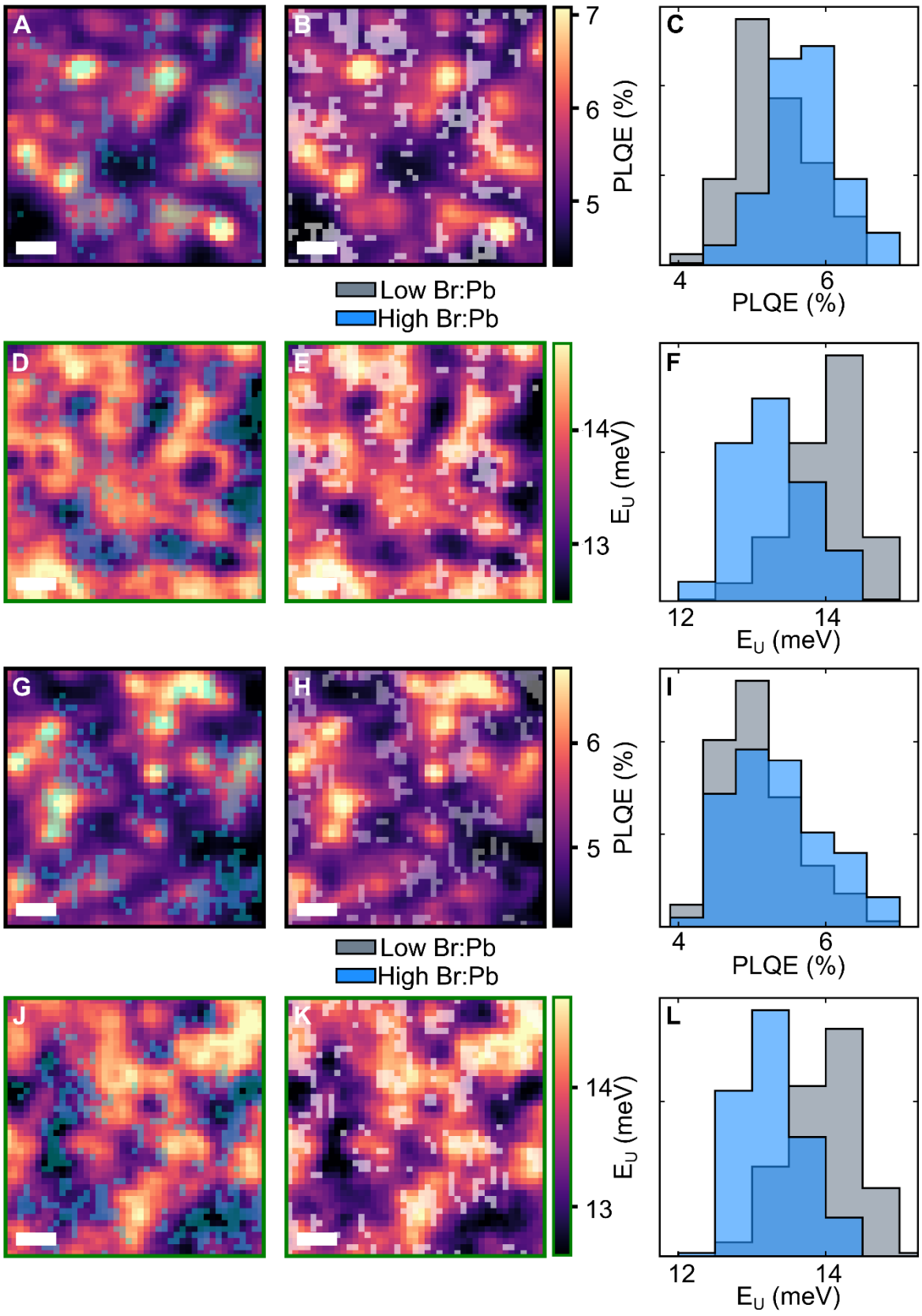


**Supplementary Figure 12: PLQE and Urbach energy maps of several regions of $FA_{0.79}MA_{0.16}Cs_{0.05}Pb(I_{0.83}Br_{0.17})_3$ triple cation perovskite films overlaid with nXRF.**

a) PLQE map overlaid with high and b) low Br:Pb regions from nXRF. c) Histogram of PLQE values from high and low Br:Pb regions. d) Urbach energy map overlaid with high and e) low Br:Pb regions from nXRF. f) Histogram of Urbach energy values from high and low Br:Pb regions. g) PLQE map of another region of a triple cation perovskite film overlaid with high and h) low Br:Pb regions from nXRF. i) Histogram of PLQE values from high and low Br:Pb regions. j) Urbach energy map overlaid with high and k) low Br:Pb regions from nXRF. l) Histogram of Urbach energy values from high and low Br:Pb regions. All scalebars are 1 μm.

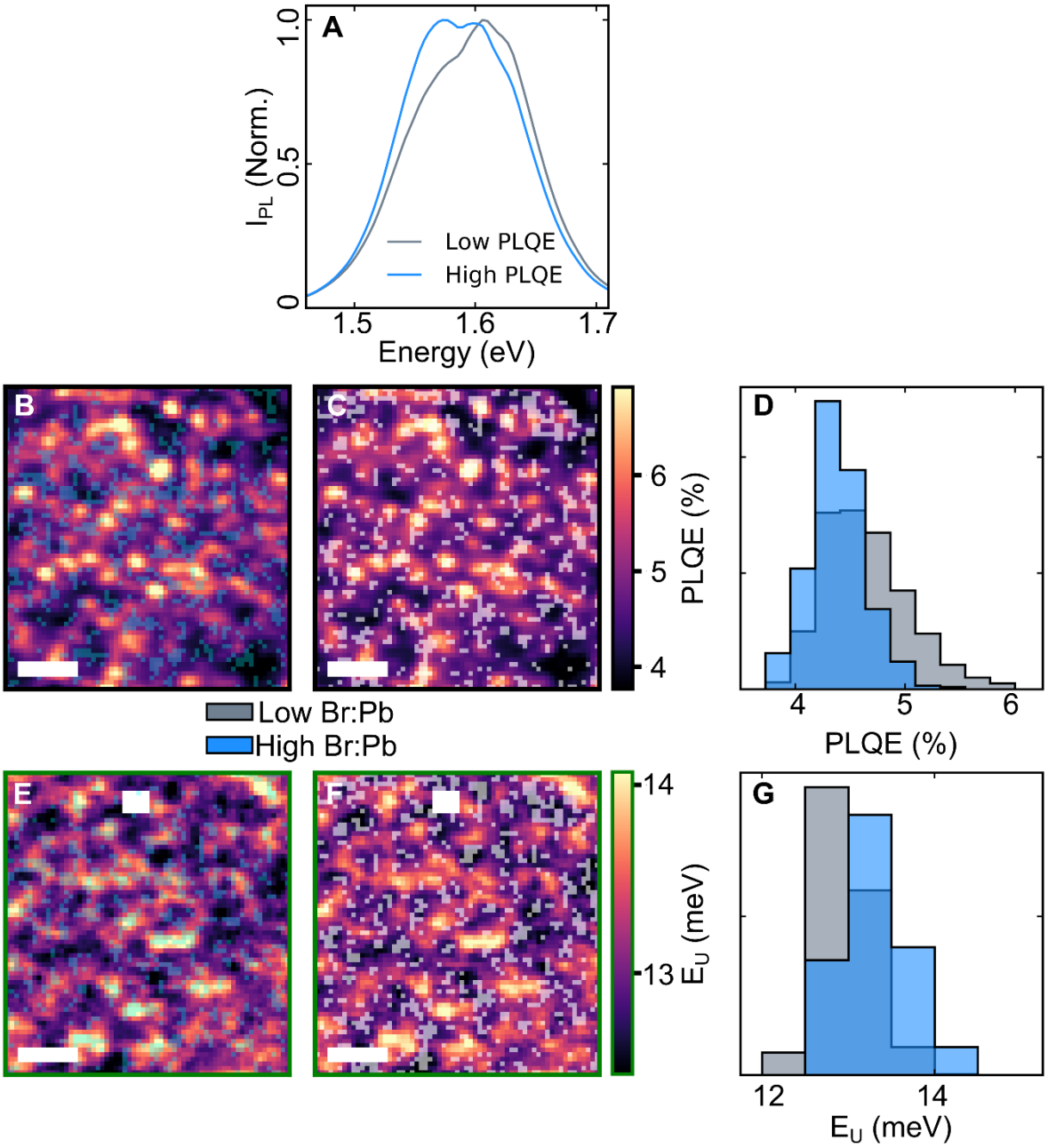


**Supplementary Figure 13: Optoelectronic and nXRF correlation in a triple cation perovskite thin film that exhibits high halide segregation.** a) PL spectra of low and high PLQE regions exhibiting very broad bimodal distributions in both cases indicating much more advanced halide segregation. b) PLQE maps overlaid with high (>80$^{th}$ percentile) and c) low(<20$^{th}$ percentile) Br:Pb regions. d) Histograms of PLQE in the high and low Br:Pb regions. e) $E_U$ maps overlaid with high (>80$^{th}$ percentile) and f) low(<20$^{th}$ percentile) Br:Pb regions. g) Histograms of $E_U$ in the high and low Br:Pb regions. These correlations show that as the segregation becomes

more severe, the nanoscale iodide domains become large enough to be detected in nXRF and the correlation begins to reverse compared to the less segregated case.

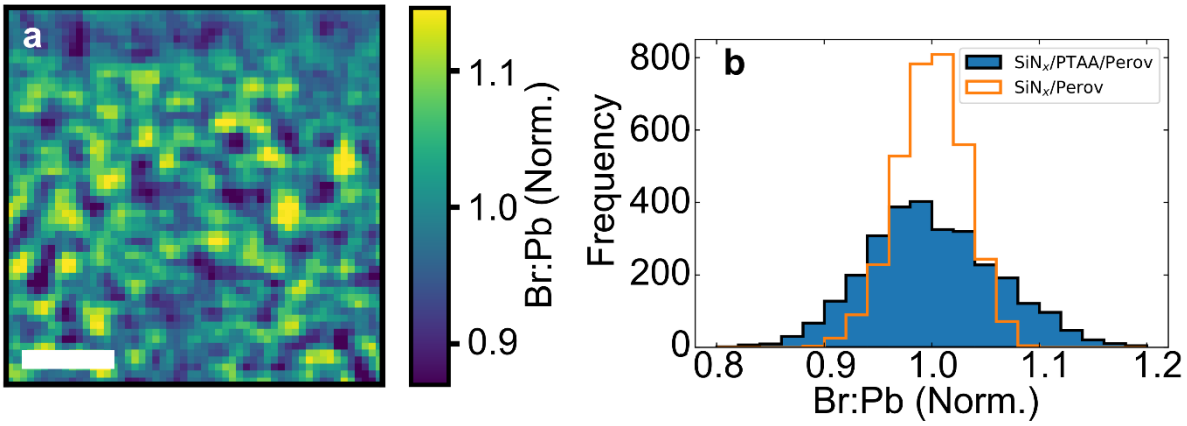


**Supplementary Figure 14: nXRF map of $FA_{0.79}MA_{0.16}Cs_{0.05}Pb(I_{0.83}Br_{0.17})_3$ film deposited on PTAA.** a) Normalised Br:Pb ratio map of $FA_{0.79}MA_{0.16}Cs_{0.05}Pb(I_{0.83}Br_{0.17})_3$ film deposited on PTAA, without any previous exposure to light. b) Histogram comparing the spread Br:Pb ratios in a $FA_{0.79}MA_{0.16}Cs_{0.05}Pb(I_{0.83}Br_{0.17})_3$ deposited directly on $SiN_x$ or on PTAA ) – the latter being employed for all other data in this work. The different distribution widths exemplify how the surface chemistry of the substrate can impact the halide chemical heterogeneity in the sample.

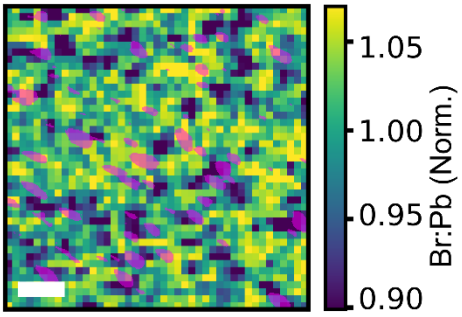


**Supplementary Figure 15. nXRF map overlaid with PEEM intensities.** nXRF map of triple cation perovskite film overlaid with PEEM spots (magenta) of the same region indicating sights of local trap states

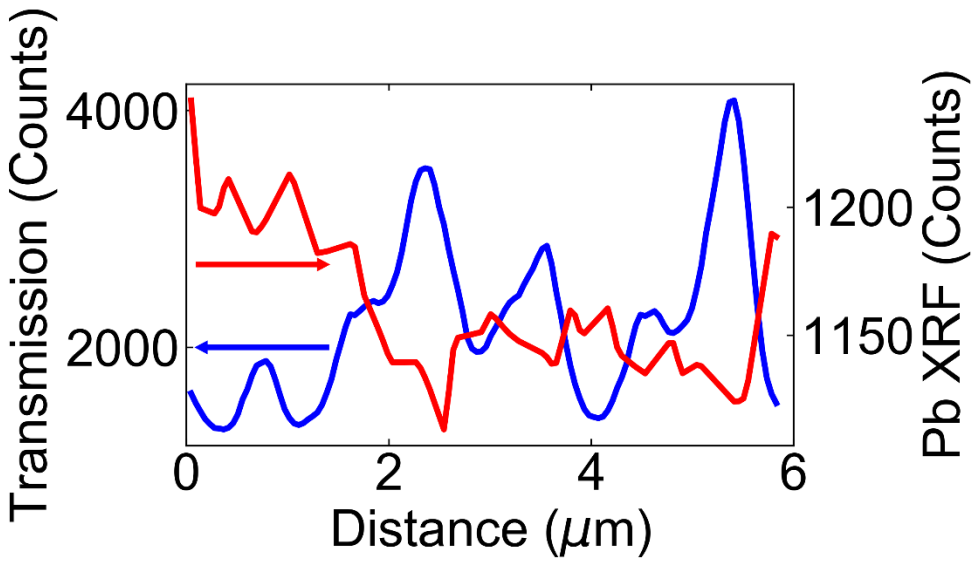


**Supplementary Figure 16: Transmission and Pb XRF correlation.** Transmission signal (blue line) and Pb XRF signal (red line) of the region used for correlation showing as the Pb signal increases, the probe transmission intensity decreases.

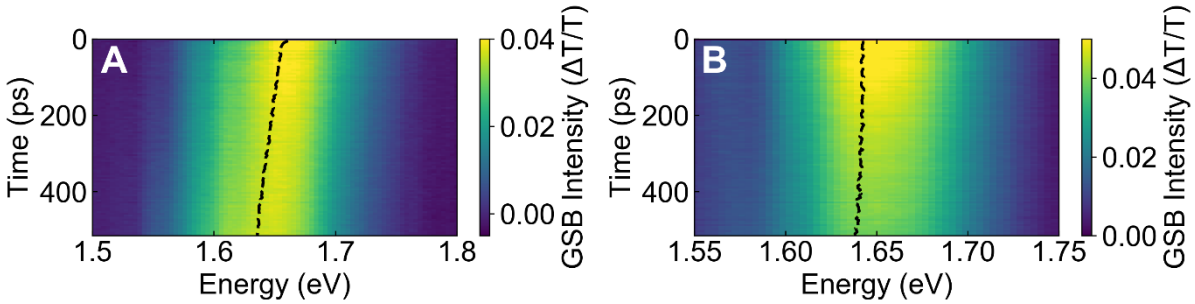


**Supplementary Figure 17: TA spectra of high and low Br regions.** (**A**) TA spectra as a function of time in the high Br and (**B**) low Br regions highlighted in the main text. Dashed lines indicate the centre of mass of the GSB as a function of time.

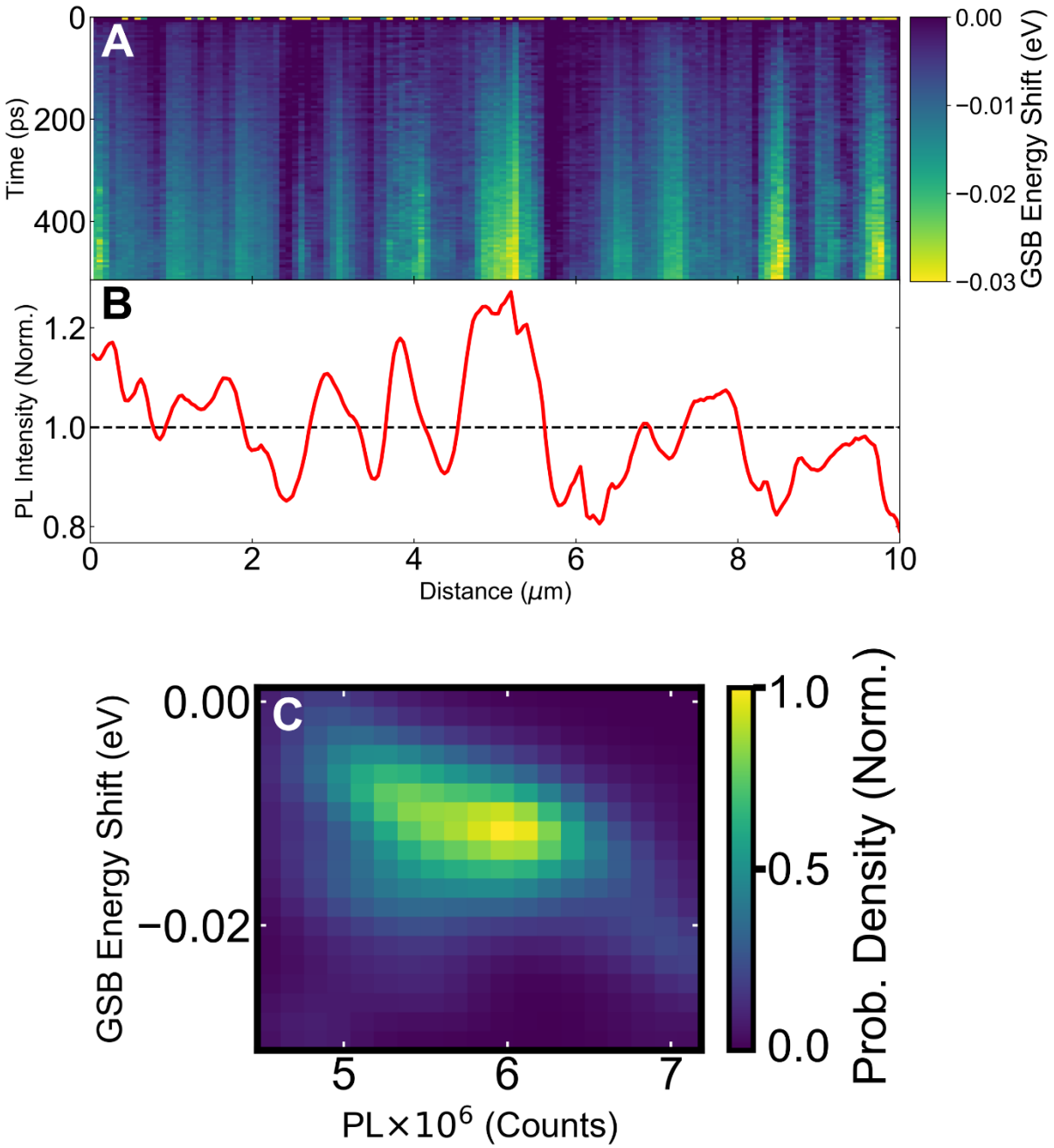


**Supplementary Figure 18: Overlay between TA GSB and PL Intensity:** (**A**) Colour map of the change in GSB energy as a function of pump probe delay time. (**B**) PL intensity (normalised to the mean of the whole line) of the same line shown in panel (A). (**C**) 2D kernel density estimation plot of the PL intensity versus the GSB energy shift showing a negative correlation suggesting red shifting carrier population is indicative of higher PL emission (Spearman's r value=-0.32, p-value << 0.0001).

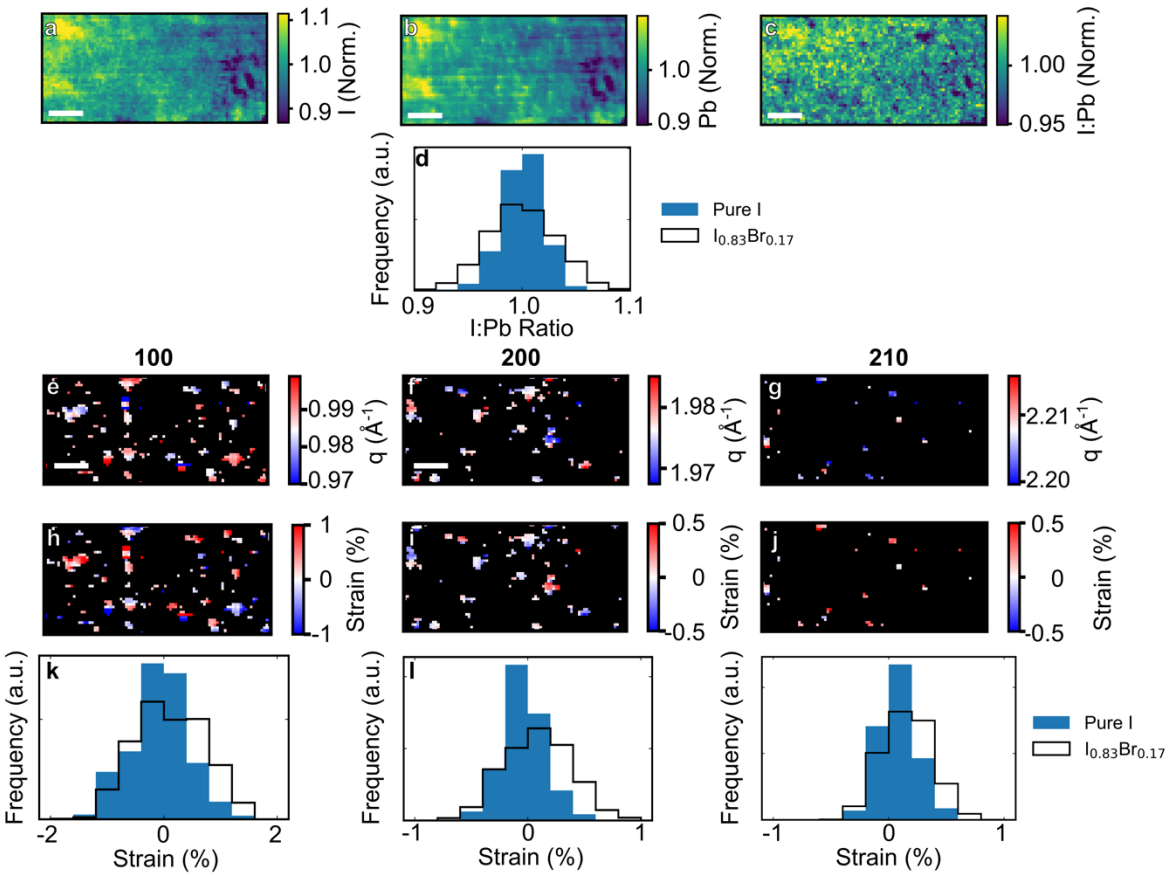


**Supplementary Figure 19: nXRF of $FA_{0.79}MA_{0.16}Cs_{0.05}PbI_3$ film.** Mean normalised a) I and b) Pb nXRF maps respectively. c) I:Pb nXRF ratio map. d) Histogram showing the distribution of I:Pb ratio across the map of a $FA_{0.79}MA_{0.16}Cs_{0.05}PbI_3$ film (blue) and overlaid with the I:Pb distribution in a $FA_{0.79}MA_{0.16}Cs_{0.05}Pb(I_{0.83}Br_{0.17})_3$ (black). nXRD peak positions of the e) 100, f) 200 and g) 210 peaks respectively. Corresponding strain distribution maps for the h) 100, i) 200 and j) 210 families of planes. Strain distribution comparison between the pure iodide samples (blue) and the mixed halide samples (black) along the k) {100}, l) {200} and m) {210} families of planes. All scalebars are 2 μm.